Multi-octave mid-infrared supercontinuum generation in tapered chalcogenide-glass rods

Esteban Serrano, Damien Bailleul, Frédéric Désévédavy, Grégory Gadret, Pierre Mathey, P. Béjot, Asuka Nakatani, Tonglei Cheng, Yasutake Ohishi, Bertrand Kibler, et al.

Multi-Octave Mid-Infrared Supercontinuum Generation in Tapered Chalcogenide-Glass Rods

ESTEBAN SERRANO,[1] DAMIEN BAILLEUL,[1] FRÉDÉRIC DÉSÉVÉDAVY,[1] GRÉGORY GADRET,[1] PIERRE MATHEY,[1] PIERRE BÉJOT,[1] ASUKA NAKATANI,[2] TONGLEI CHENG,[2] YASUKATE OHISHI,[2] BERTRAND KIBLER,[1,*] AND FRÉDÉRIC SMEKTALA[1]

[1] *Laboratoire Interdisciplinaire Carnot de Bourgogne, UMR6303 CNRS-UBFC, Dijon, France*
[2] *Research Center for Advanced Photon Technology, Toyota Technological Institute, Nagoya, Japan*
**Corresponding author: bertrand.kibler@u-bourgogne.fr*

Received XX Month XXXX; revised XX Month, XXXX; accepted XX Month XXXX; posted XX Month XXXX (Doc. ID XXXXX); published XX Month XXXX

We report on the experimental development of short tapered chalcogenide glass rods for mid-infrared supercontinuum generation. Multi-octave spectral broadening of femtosecond laser pulses is demonstrated from 1.7 to 16 µm in a 5-cm-long tapered $Ge_{20}Se_{70}Te_{10}$ rod with a waist diameter of 25 µm. Despite the multimode nature of the optical waveguide used, this work clearly shows the potential of such simple post-processed rods for advancing fiber SC sources with infrared glasses thereby unlocking new possibilities in terms of coupling efficiency, spectral coverage, and output power.

Supercontinuum (SC) generation has been intensively studied in various optical fibers. During the last decade, the interest has significantly shifted toward the mid-infrared (mid-IR) spectral region where molecules display fundamental vibration absorptions [1–3]. Among infrared glasses, chalcogenides exhibit suitable transparency that makes them the best candidate for fiber-based SC sources covering the mid-IR spectrum (2-20 µm). However, the ability to handle high-quality glasses and fiber drawing to fabricate engineered low-loss fibers for SC generation beyond 12 µm is very challenging [4–7]. Chalcogenide (ChG) fibers have generally their zero-dispersion wavelength (ZDW) considerably far located from the near-infrared region, specifically in the range of 5-10 µm. This raises a challenge when considering the lack of high-power and compact laser sources in this spectral range, prompting extensive experimental efforts to focus on fibers with shifted ZDW [3,8,9]. Nevertheless, recent advances of tunable high peak-power laser sources based on optical parametric amplifiers (OPAs) and difference-frequency generation (DFG) modules have enabled significant breakthroughs in terms of supercontinuum extension and power spectral density towards the mid-IR [8–10].

In this letter, we experimentally demonstrate multi-octave mid-IR SC generation in a 5-cm-long tapered chalcogenide-glass rod. Fiber tapering is a widely recognized post-processing technology that offers efficient management of light confinement and dispersion [10–12]. It can be also considered as a simpler, faster and cost-efficient alternative to the fabrication of step-index, double-clad or microstructured fibers, in particular for chalcogenide glasses, and when a single-index glass rod is used as follows. Tapered fibers have been already used in the literature for SC generation but always considering structured fibers, namely with a step-index or more complex index profiles [13–15]. Optimized spectral broadening has been demonstrated in the mid-IR by means of this technique while at the same time achieving high output powers, for example, by Petersen et al. [16] with tapered microstructured fibers, as well by Hudson et al. [17] with tapered step-index fibers. In both cases, the achieved SC output power exceeds 30 mW, while the SC spectrum spans over 10 µm. In general, SC experiments were carried out within single-mode or few-mode fibers. More recently, other works have been performed with large-core multimode fibers in order to significantly reduce the coupling difficulty as well as endure higher power [18,19].

The glass compositions used in this work belong to the Ge-Se-Te (GST) ternary system. The Se-rich part of the pseudo-binary $GeSe_4$-$GeTe_4$ is chosen to ensure compatibility with fiber technology. We have already reported on the synthesis and the purification process of Ge-Se-Te glasses in our previous works [4,9,20]. For this study, a $Ge_{20}Se_{70}Te_{10}$ glass preform is synthesized by the standard melt quenching method. Our purification process allows the absorption bands to be reduced considerably, in particular the O- and H- bonds. The losses therefore have a negligible continuous background between 2 and 11 µm (below 0.06 dB/cm). The 16-mm outer diameter initial preform is then drawn to a long (several meters) and thin optical rod of 180 µm. The low losses of the resulting single-index rod are depicted in Fig. 1(a). Only the combined absorptions of O- bonds remain visible between 12 and 14 µm for short cm-long fiber segments (see Fig.1 (a)). The wavelength-dependent refractive indices for the glass used was calculated based on the Clausius-Mossoti relation and refractive index measurements [20]. The dispersive and nonlinear properties of the scalar fundamental mode of the single-index rods

were calculated for different diameters from 180 down to 25 µm. As a basic assumption, we consider the taper to have a circular cross-section with an infinite air cladding. Given the high refractive index of GST glass (beyond 2.4),

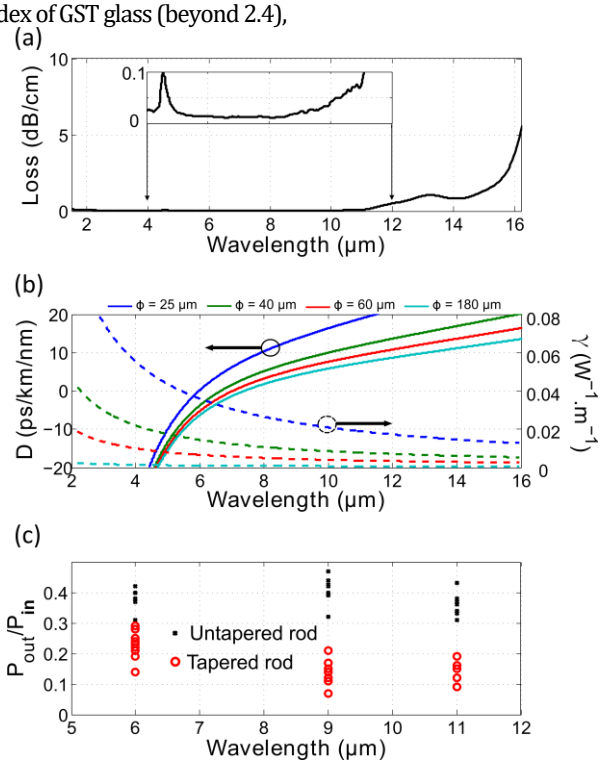

Fig. 1. (a) Measured losses of the $Ge_{20}Se_{70}Te_{10}$ fiber. (b) Left axis, solid line curves: Calculated dispersion profile D of fundamental guided mode for GST rod diameter of Ø = 25, 40, 60 and 180 µm. Right axis, dashed curves: Calculated wavelength-dependent curves of rod nonlinear coefficient for the same diameters. (c) Ratio of the output power to the incoming power for the untapered-rod and for the 25-µm tapered rod.

the fundamental mode remains well confined into the rod for all the diameters under study. Figure 1(b) shows the corresponding dispersion curves. As expected, the 180-µm diameter rod exhibits similar dispersion properties as the bulk material. The zero-dispersion wavelength (ZDW) is close to 7.1 µm. When decreasing significantly the diameter of the rod down to 25 µm, the ZDW becomes shifted toward shorter wavelengths, nearly about 5.7 µm. The nonlinear coefficient γ associated to the calculated fundamental mode is also shown (right axis) for the different wavelengths and outer diameters according to the relation $\gamma = 2\pi n_2/(\lambda A_{\text{eff}})$, where λ is the laser wavelength, A_{eff} the effective mode area, and $n_2 = 8.2 \times 10^{-18}$ m^2/W is the nonlinear index of our glass [21]. This nonlinear coefficient strongly increases for reduced rod diameters. For example, at 6-µm wavelength, the nonlinearity is 50 times higher for 25-µm rod than for initial 180-µm rod. From this simple analysis of modal properties, it then appears that the shift of ZDW as well as the increased light confinement into a tapered rod will positively impact SC generation in terms of bandwidth compared to untapered rods. To fabricate short adiabatic biconical tapers from our 180-µm single-index rod, a well-known post-processing technique was used based on the VYTRAN Glass Processing Workstation (GPX-3400). Fusion splicing and tapering of specialty fibers can be executed by the glass processing platform, which incorporates a suitable filament heater, precision stages with multi-axis control, and high-resolution CCD imaging system.

Here, we investigated rod tapering with smooth transition regions from the 180-µm rod diameter to the waist and back to the initial rod diameter. In order to estimate the coupling efficiency and losses induced by the tapered section, we measured the full transmission of several samples of 5-cm-long tapered and untapered GST rods at a few mid-IR wavelengths. Light coupling was obtained by means of a 25-mm focal length lens. Corresponding results are shown in Fig. 1 (c). On the first hand, one can notice the high transmission and then coupling ratio that can be obtained in untapered rods approaching 50% (this includes coupling efficiency and Fresnel reflections). On the other hand, there is nearly 2-3 dB increase of induced-loss for rods including a taper section. As in the current configuration, the coupling was optimized without taking care about the number of modes excited (i.e., multimode propagation), such additional losses can be first attributed to the excitation of higher-order modes that are not guided after, and filtered out in the taper section. For instance, the number of guided linearly polarized (LP_{0m}) modes (with circular symmetry) is reduced by a factor of 7 in the taper at 6-µm wavelength. However, it can be also presumed that the profile of the taper or any surface defects cause transmission losses on higher-order modes [22]. Indeed, we have checked that the full transmission measured can be strongly dependent on the initial coupling.

The efficiency of tapered GST rods for mid-IR SC generation was assessed by using the experimental setup depicted in Fig.2. The mid-IR pump pulses was provided by using a Ti:Sapphire laser amplifier system at 1-kHz repetition rate combined with an optical parametric amplifier (OPA) and a difference-frequency-generation (DFG) module. The resulting pulses exhibit a 170-fs width and a central wavelength tunable from 2.5 to 11 µm. The available energy at 6.3-µm wavelength was about 4 µJ. Next, mid-IR pulses are coupled into our GST rods by means of a Ge lens. The SC signal at the rod output was collected by a butt-coupled 1-m-long hollow-core fiber with an internal diameter of 1 mm. The latter exhibits high transmission over the 2-16 µm spectral range. The collected light is launched into a monochromator coupled to a MCT detector operating up to 22 µm. Different diffraction gratings were used to cover the 1-22 µm spectral range. In order to remove the high-order diffraction peaks from the gratings, several long-pass filters were used. Moreover, the spatial distribution of output SC was also characterized by near-field imaging of the rod end-face onto beam profiling camera operating from 2 to 16 µm. The average power for each SC was measured by means of a thermal power sensor.

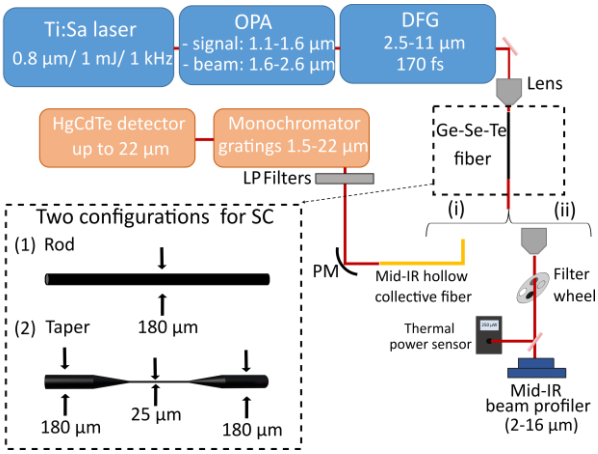

Fig. 2. Experimental setup for mid-IR SC generation, either with untapered (1) or tapered (2) GST rod. Output SC is characterized via (i) a monochromator coupled to a MCT detector and (ii) near-field imaging with a beam profiling camera.

First, it is worth to mention that finding the optimal coupling condition is crucial in such multimode glass rods. The nonlinear pulse propagation is known to be strongly dependent on spatiotemporal couplings in multimode waveguides [23]. To maximize spectral broadening while controlling the spatial content of the generated SC, one has to favor initial coupling into the fundamental mode of the waveguide, thus allowing adiabatic change of the mode and minimizing energy loss. In such a case, this prevents from detrimental effects such as the numerous intermodal couplings with low modal overlapping for nonlinear effects, and the filtering of higher-order modes becoming non-guided inside the tapered section. But even in this ideal case of fundamental mode excitation combined with the femtosecond regime and short propagation, one can observe spontaneous intermodal phase-matching, namely related to the phenomenon of discretized conical emission [24-25], when using input peak powers close to the critical self-focusing threshold. The detailed characterization of nonlinear spatiotemporal dynamics is beyond the scope of this letter, however, we provide some experimental findings that confirm the above simple guidelines.

As a first example, we have checked the impact of focal length of the coupling lens on the output SC bandwidth. Figure 3(b) reports the SC recorded for a tapered GST with 25-µm diameter when using two Ge lenses with 12- and 15-mm focal length. Here, the corresponding taper profile, measured in Fig. 3(a), exhibits transition lengths of 10 mm, and a waist length of 30 mm. Increasing the focal length to 15 mm helps to optimize the coupling into the fundamental mode whose diameter is about 84 µm. Optimal tapering parameters for SC generation were carried out on different rods with varying waist diameters and transition lengths that can be reached by means of our glass processing workstation (the maximum length of the tapered section including transitions and waist is limited to 100 mm). Typically, a tapering factor up to 1/12 can be reached onto the rod diameter with a maximum 80-mm-long waist region, while preserving efficient transmission. Asymmetric transition regions were also investigated without noticing a relevant impact for our SC experiments. Figure 3(c) illustrates the impact of waist size on SC bandwidth through the comparison of two tapered GST rods with 15- and 25-µm waist diameters. We clearly observe that the spectral broadening is stronger in the 15-µm waist taper, in particular due to the stronger mode confinement and higher nonlinearity. Nevertheless, such small waist diameters were subject to irreversible high-power damages and degradation issues. To optimize spectral broadening with the mid-IR laser beam used, a tapered rod with transitions of 12.5 mm and a 25-mm-long waist region with a diameter of 25 µm was obtained.

It was possible to easily achieve SC generation in both the untapered and the tapered Ge-Se-Te rods. Figure 4 presents both spectra recorded experimentally for the same input pulse energy. For the untapered rod shown in Fig. 4(a), the SC spans from 2.5 to 12.5 µm, and the energy measured at the output was about 0.36 µJ. Indeed, we found that the optimal pump wavelength for SC generation is 6.3 µm as pulse energy from the DFG module strongly decreases with wavelength. Given the high peak power coupled into the fiber, even in the normal dispersion regime, self-phase modulation efficiently generates a SC wide enough to cross the ZDW

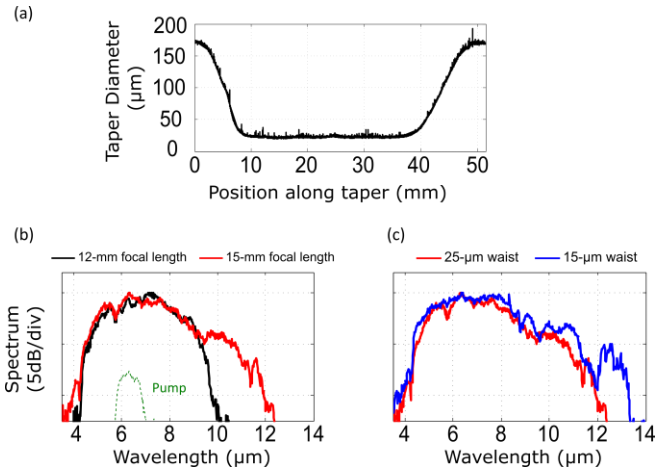

Fig. 3. (a) Measured diameter of the 25-µm waist taper with transition lengths of 10 mm and a waist length of 30 mm. (b) Measured output SC for the 5-cm-long segment of tapered rod, pumped at 6.3 µm by means of two coupling lenses with focal length of 12 mm (black solid line) or 15 mm (red solid line). (c) Spectra obtained with coupling lens ($f = 15$ mm) in the 25-µm waist taper (red solid line) and the 15-µm waist taper (blue solid line). The input pump spectrum (green dashed line) is also depicted in subplot(b).

and favor the spontaneous emergence of phase-matched dispersive waves to cover the spectral region between 2.5 and 12.5 µm [25]. In this case, the generated SC is obtained by pumping in the normal dispersion regime (i.e. ZDW ~ 7.2 µm). For the tapered glass rod with a waist diameter of 25 µm, the resulting SC spectrum extends from 1.7 to 16 µm as shown in Fig. 4(b). The corresponding output energy is 0.16 µJ, only twice less than its untapered counterpart. We clearly observe the strong enhancement of SC generation on both edges of the spectrum in our Ge-Se-Te glass rod by using our tapering design. The spectral bandwidth is increased by ~ 26 THz at the near-IR edge and by 4

THz at the mid-IR edge, thus offering a ~ 160 THz bandwidth mid-IR SC source. The improved confinement in the waist region combined with the tuning of ZDW back and forth the pump wavelength facilitate spectral broadening and flattening of the SC. We also characterized the power spectral density by filtering some broadband wavelength windows of interest (see Fig. 4(c-d)). The energy distribution over the spectral edges appears to be increased between untapered and tapered rods through additional frequency conversions. In the tapered rod, a significant energy conversion, nearly 20% of the transmitted one, is delivered beyond 10 µm. Although it is difficult to describe the modal content precisely with our near-field measurements, we note a cleaning of SC spatial profile at the output of the tapered rod over all the spectral ranges, as confirmed by the comparison of inset plots in Fig. 4. This may result from higher-order mode filtering in the tapered section of our GST rod.

In summary, our findings hold great significance as they demonstrate the feasibility of producing multi-octave mid-IR SC spanning from 1.7 to 16 µm in a 5-cm long highly-multimode tapered chalcogenide rod. To the best of our knowledge, this first SC demonstration in tapered rods might trigger new opportunities for chalcogenides into the mid-IR domain and beyond. By surpassing the limitations associated with step-index or microstructured fibers, such as low damage threshold and power coupling restrictions, these devices offer a promising alternative. Using tapered rods with MHz laser chains could allow spectra to be obtained on such large mid-IR bandwidths combined with high average power. It is important to mention that the output beam profile still exhibits a multimode behaviour, which could present limitations for specific applications. However, future works conducting a more-in-depth analysis and control of the spectral and modal content could help in overcoming this challenge.

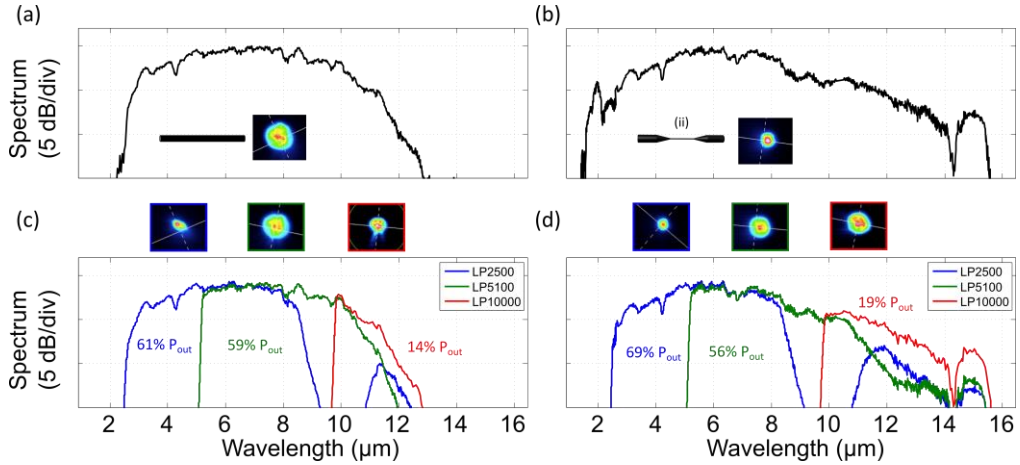

Fig. 4. Measured output SC spectra pumped at 6.3 µm for 5-cm-long segments of (a,c) untapered and (b,d) tapered rods. (a,b) Full measured spectra. Insets show the near-field image of full SC light at the rod end-face. (c,d) Spectra obtained after using specific mid-IR filters. The SC power distribution as a function of spectral ranges is also given. Near-field images were also characterized for the different spectral ranges of the filters (see top insets in subplots c and d). Note the quality of rod end faces through manual cleaving process by a scalpel blade may impact the spatial profiles shown in the insets.

Funding. CNRS International emerging action (IEA). Agence Nationale de la Recherche (EQUIPEX+ contract ANR-21-ESRE-0040) and the Bourgogne Franche-Comté region.

Disclosures. The authors declare no conflicts of interest.

Data availability. Data underlying the results presented in this paper are not publicly available at this time but may be obtained from the authors upon reasonable request.

References

1. Y. Ohishi, Opt. Mater. Express **12**, 3990 (2022).
2. T. Sylvestre, E. Genier, A. N. Ghosh, P. Bowen, G. Genty, J. Troles, A. Mussot, A. Peacock, M. Klimczak, A. Heidt, J. Travers, O. Bang, and J. Dudley, J. Opt. Soc. Am. B (2021).
3. S. Dai, Y. Wang, X. Peng, P. Zhang, X. Wang, and Y. Xu, Applied Sciences **8**, 707 (2018).
4. A. Lemière, R. Bizot, F. Désévédavy, G. Gadret, J.-C. Jules, P. Mathey, C. Aquilina, P. Béjot, F. Billard, O. Faucher, B. Kibler, and F. Smektala, Results in Physics **26**, 104397 (2021).
5. T. Cheng, K. Nagasaka, T. H. Tuan, X. Xue, M. Matsumoto, H. Tezuka, T. Suzuki, and Y. Ohishi, Opt. Lett. **41**, 2117 (2016).
6. Z. Zhao, B. Wu, X. Wang, Z. Pan, Z. Liu, P. Zhang, X. Shen, Q. Nie, S. Dai, and R. Wang, Laser & Photonics Reviews **11**, 1700005 (2017).
7. C. R. Petersen, U. Møller, I. Kubat, B. Zhou, S. Dupont, J. Ramsay, T. Benson, S. Sujecki, N. Abdel-Moneim, Z. Tang, D. Furniss, A. Seddon, and O. Bang, Nature Photon **8**, 830 (2014).
8. U. Møller, Y. Yu, I. Kubat, C. R. Petersen, X. Gai, L. Brilland, D. Méchin, C. Caillaud, J. Troles, B. Luther-Davies, and O. Bang, Opt. Express **23**, 3282 (2015).
9. B. Kibler, E. Serrano, A. Maldonado, L.-R. Robichaud, S. Duval, M. Bernier, R. Bizot, F. Désévédavy, R. Vallée, Y. Messaddeq, and F. Smektala, Optics Communications 129568 (2023).
10. B. Luo, Y. Wang, Y. Sun, S. Dai, P. Yang, P. Zhang, X. Wang, F. Chen, and R. Wang, Infrared Physics & Technology **80**, 105 (2017).
11. S. W. Harun, K. S. Lim, C. K. Tio, K. Dimyati, and H. Ahmad, Optik **124**, 538 (2013).

12. Y. Sun, S. Dai, P. Zhang, X. Wang, Y. Xu, Z. Liu, F. Chen, Y. Wu, Y. Zhang, R. Wang, and G. Tao, Opt. Express **23**, 23472 (2015).
13. N. Zhang, X. Peng, Y. Wang, S. Dai, Y. Yuan, J. Su, G. Li, P. Zhang, P. Yang, and X. Wang, Opt. Express **27**, 10311 (2019).
14. Y. Wang, S. Dai, G. Li, D. Xu, C. You, X. Han, P. Zhang, X. Wang, and P. Xu, Opt. Lett. **42**, 3458 (2017).
15. C. R. Petersen, M. B. Lotz, G. Woyessa, A. N. Ghosh, T. Sylvestre, L. Brilland, J. Troles, M. H. Jakobsen, R. Taboryski, and O. Bang, Opt. Lett. **44**, 5505 (2019).
16. C. R. Petersen, R. D. Engelsholm, C. Markos, L. Brilland, C. Caillaud, J. Trolès, and O. Bang, Opt. Express **25**, 15336 (2017).
17. D. D. Hudson, S. Antipov, L. Li, I. Alamgir, T. Hu, M. E. Amraoui, Y. Messaddeq, M. Rochette, S. D. Jackson, and A. Fuerbach, Optica **4**, 1163 (2017).
18. Z. Eslami, P. Ryczkowski, C. Amiot, L. Salmela, and G. Genty, J. Opt. Soc. Am. B **36**, A72 (2019).
19. Z. Eslami, P. Ryczkowski, L. Salmela, and G. Genty, Opt. Lett. **45**, 3103 (2020).
20. A. Lemière, F. Désévédavy, P. Mathey, P. Froidevaux, G. Gadret, J.-C. Jules, C. Aquilina, B. Kibler, P. Béjot, F. Billard, O. Faucher, and F. Smektala, J. Opt. Soc. Am. B **36**, A183 (2019).
21. L. Sun, F. Chen, Y. Xu, Y. Huang, S. Liu, Z. Zhao, X. Wang, P. Zhang, S. Dai, and X. Zhang, Appl. Phys. A **122**, 816 (2016).
22. S. Ravets, J. E. Hoffman, P. R. Kordell, J. D. Wong-Campos, S. L. Rolston, and L. A. Orozco, J. Opt. Soc. Am. A **30**, 2361 (2013).
23. K. Krupa, A. Tonello, A. Barthélémy, T. Mansuryan, V. Couderc, G. Millot, P. Grelu, D. Modotto, S. A. Babin, and S. Wabnitz, APL Photonics **4**, 110901 (2019).
24. B. Kibler and P. Béjot, Phys. Rev. Lett. **126**, 023902 (2021).
25. K. Stefańska, P. Béjot, K. Tarnowski, and B. Kibler, ACS Photonics **10**, 727 (2023).